3.5 Spatial Closure based on the HO Solution

This sections describes an alternative spatial closure to the LO equations based on a parametric relation from the HO solution. In addition to estimating the angular consistency terms, the HO intensity estimates a relation between volume and face-averaged intensities to eliminate the remaining unknowns from the equations. In the remainder of this section, we will motivate the HO spatial closure by manipulating a half-range balance equations to form a single unknown for each cell and half range. We will then discuss the forms of HO spatial closures investigated, based on modifications to standard spatial closures.

3.5.1 Motivation

A half-range balance equation for $\mu > 0$ is formed by adding the exact L and R radiation moment equations given by Eq. (3.18) and (3.19), i.e.,

$$\mu^+_{i+1/2}\phi^+_{i+1/2} - \mu^+_{i-1/2}\phi^+_{i-1/2} + \sigma_{a,i}h_i\phi^+_i = \frac{h_i}{2}q_i, \tag{3.27}$$

where q_i represents the cell-averaged emission source. In the HOLO algorithm, after estimating the consistency terms $\mu^+_{i\pm1/2}$ upwinding the inflow term $\phi^+_{i-1/2}$, an additional equation is needed to eliminate the outflow $\phi^+_{i+1/2}$ to produce an equation for a single unknown ϕ^+_i. Standard spatial discretizations techniques use a fixed approximation for all cells to eliminate the outflow in terms of other unknowns. Alternatively, the HO solution can be used to estimate a parametric relation between the other unknowns and the outflow, i.e.,

$$\phi^+_{i+1/2} = f(\gamma_i^{+,HO}, \phi^+_i, \phi^+_{x,i}, \phi^+_{i-1/2}), \tag{3.28}$$

where $\gamma_i^{HO,+}$ is a local constant to be estimated with the HO solution and f is some function of some number of the input variables. The ECMC solution can provide all of the unknowns in the above equation, so the value of γ_i^{HO} can be determined directly.

If the problem were linear, or the nonlinear problem was fully converged, then application of this closure can ensure that the HO and LO equations produce the same moments, preserving the HO accuracy. To produce the same moments, the HO solution must also satisfy the local balance equation, e.g., Eq. (3.27). Then the LO equations and HO equations must have the same moments to satisfy both Eq. (3.28) and Eq. (3.27), upon nonlinear convergence of the outer HOLO iterations. If any higher moments are introduced through the spatial closure, then the HO solution must also satisfy the corresponding balance equations that the LO equations do. For example, both the LO and HO equation must satisfy the first moment equation in space if the closure is a function of the first moment.

As TRT problems are non-linear (i.e., scattering or thermal emission are included in q), the moments will only be preserved upon non-linear convergence of the source. The nonlinearity introduces the possibility for stability issues, particularly with MC noise. However, we have already consistently formed angular consistency terms, so the the spatial closure should be more stable than introducing other terms, such as in NDA methods [41, 40].

3.5.2 Choice of Spatial Closure

We will explore two different closure relations based on modifications to the standard LD closure: a scaled slope, i.e.,

$$\phi^{\pm}_{i\pm1/2} = \phi^{+}_{i} \pm \gamma^{\pm}_{i}\phi^{+}_{x,i} \tag{3.29}$$

and a scaled average

$$\phi^{\pm}_{i\pm1/2} = \gamma^{\pm}_i \phi^{+}_i \pm \phi^{+}_{x,i}, \tag{3.30}$$

where a value of $\gamma_i = 1$ produces the standard linear discontinuous expressions for the extrapolated outflows. Our LO system is formulated in terms of L and R moments, rather than the average and slope. Thus, Eq. (3.29) and (3.30) are expressed in terms of the L and R unknowns, using the relations given in App. A.1. In terms of these moments, the scaled-slope closure is

$$\phi^{+}_{i+1/2} = \left(\frac{1-3\gamma^{+}_i}{2}\right)\langle\phi\rangle^{+}_{L,i} + \left(\frac{1+3\gamma^{+}_i}{2}\right)\langle\phi\rangle^{+}_{R,i} \tag{3.31}$$

$$\phi^{-}_{i-1/2} = \left(\frac{1+3\gamma^{-}_i}{2}\right)\langle\phi\rangle^{-}_{L,i} + \left(\frac{1-3\gamma^{-}_i}{2}\right)\langle\phi\rangle^{-}_{R,i} \tag{3.32}$$

and the scaled-average relation is

$$\phi^{+}_{i+1/2} = \left(\frac{\gamma^{+}_i-3}{2}\right)\langle\phi\rangle^{+}_{L,i} + \left(\frac{\gamma^{+}_i+3}{2}\right)\langle\phi\rangle^{+}_{R,i} \tag{3.33}$$

$$\phi^{-}_{i-1/2} = \left(\frac{\gamma^{-}_i+3}{2}\right)\langle\phi\rangle^{-}_{L,i} + \left(\frac{\gamma^{-}_i-3}{2}\right)\langle\phi\rangle^{-}_{R,i}. \tag{3.34}$$

The HO solution is used to estimate γ_i. The MC solution must be modified to tally the MC estimated intensity on faces. For example, for $\mu > 0$, the LO equations for moments at $k+1$ use closure parameters evaluated at $k+1/2$ as

$$\gamma^{+,HO,k+1/2}_i = \frac{\phi^{+,HO,k+1/2}_{i+1/2} - \phi^{+,HO,k+1/2}_i}{\phi^{+,HO,k+1/2}_{x,i}}, \tag{3.35}$$

for the scaled-slope closure. For this closure, as the slope goes to zero this expression becomes undefined. In cells where the slope is $O(10^{-13}\psi_i)$, we use $\gamma_i = 1$. For the problems tested, no issues have occurred with this closure, even γ can become very

large for common, small values of $|\psi^x/\psi_i|$. This is because in such regions the solution is changing minimally anyways. The main benefit of the scaled-slope closure is it allows for values of γ that are equivalent to other closures, as discussed in App. A.1: $\gamma_i = 0$ produces a step closure [21], which has a zero slope over the cell, and $\gamma_i = 1/3$ produces a lumping-equivalent closure.

3.5.3 The Doubly-Discontinuous Trial Space

Because of the temperature unknowns and the HO scattering source representation, a representation on the interior of the cell for the temperature and intensity is needed. Thus, we introduce a linear doubly discontinuous (LDD) trial space for the half-range intensities, which is depicted in Fig. 3.3. The linear relation on the interior of the cell preserves the L and R moments of the solution, and the outflow from the cell is some parametric (i.e., non linear) extrapolation of those moments. The temperature is still represented with a linear interpolant of T^4 and T. This trial space has an extra unknown in the radiation equations for each cell and direction, which is eliminated from the system with the HO spatial closure. The ECMC algorithm is modified to also include a LDD trial space which allows for estimate of the solution at faces, as discussed later in Sec 4.5.

To solve the LO equations, Eq. (3.31) or (3.33) is substituted locally for the appropriate outflow face term in each LO moment equation. There is a spatial closure parameter for each half-range, for each cell. The $\gamma_i^{\pm}$ are estimated from the previous HO solution. For the initial LO solve within each time step, the outflow is assumed continuous, using the standard upwinding and LD closure. As an example, the positive half-range and L moment equation (i.e., Eq. (3.18)), for the scaled-slope closure, becomes

$$
\begin{aligned}
-2\mu_{i-1/2}^{n+1,+}\left[\left(\frac{1-3\gamma_{i-1}^{HO,+}}{2}\right)\langle\phi\rangle_{L,i-1}^{+}+\left(\frac{1+3\gamma_{i-1}^{HO,+}}{2}\right)\langle\phi\rangle_{R,i-1}^{+}\right] \\
+\{\mu\}_{L,i}^{n+1,+}\langle\phi\rangle_{L,i}^{n+1,+}+\{\mu\}_{R,i}^{n+1,+}\langle\phi\rangle_{R,i}^{n+1,+} \\
+\left(\sigma_{t,i}^{n+1}+\frac{1}{c\Delta t}\right)h_i\langle\phi\rangle_{L,i}^{n+1,+}-\frac{\sigma_{s,i}h_i}{2}\left(\langle\phi\rangle_{L,i}^{n+1,+}+\langle\phi\rangle_{L,i}^{n+1,-}\right) \\
=\frac{h_i}{2}\langle\sigma_a^{n+1}acT^{n+1,4}\rangle_{L,i}+\frac{h_i}{c\Delta t}\langle\phi\rangle_{L,i}^{n,+}, \quad (3.36)
\end{aligned}
$$

and the R moment equation becomes

$$
\begin{aligned}
2\mu_{i+1/2}^{n+1,+}\left[\left(\frac{1-3\gamma_{i}^{HO,+}}{2}\right)\langle\phi\rangle_{L,i}^{+}+\left(\frac{1+3\gamma_{i}^{HO,+}}{2}\right)\langle\phi\rangle_{R,i}^{+}\right] \\
-\{\mu\}_{L,i}^{n+1,+}\langle\phi\rangle_{L,i}^{n+1,+}-\{\mu\}_{R,i}^{n+1,+}\langle\phi\rangle_{R,i}^{n+1,+}+\left(\sigma_{t,i}^{n+1}+\frac{1}{c\Delta t}\right)h_i\langle\phi\rangle_{R,i}^{n+1,+} \\
-\frac{\sigma_{s,i}h_i}{2}\left(\langle\phi\rangle_{R,i}^{n+1,+}+\langle\phi\rangle_{R,i}^{n+1,-}\right)=\frac{h_i}{2}\langle\sigma_a^{n+1}acT^{n+1,4}\rangle_{R,i}+\frac{h_i}{c\Delta t}\langle\phi\rangle_{R,i}^{n,+}. \quad (3.37)
\end{aligned}
$$

These equations contain only the original desired radiation moment and LD temperature unknowns. During the Newton solve, once new half-range intensities are determined, the temperatures are updated using the same material energy equations as for the LD closure, i.e., Eq. (3.22) and Eq. (3.23).

Because the outflow from one cell is upwinded into the next cell, energy conservation by the LO equations is preserved. The closed equations have the same numerical complexity as the LDFE LO equations, but with an increased storage on the coarse mesh for the $\{\gamma_i\}$. Also, the linear representation for the interior solutions and emission source should approach the LD closure in the equilibrium diffusion limit, as long as the HO spatial closure is estimated with sufficient statistical accuracy.

3.5.3.1 Fixups for Negative Solutions

In the case of strong gradients, the interior representation could be driven negative. In such cases, we can use the lumping-equivalent relation from App. A.1 to define the linear representation. For example, the lumped emission source is

$$T = \langle T \rangle_{L,i}^4 b_{L,i}(x) + \langle T \rangle_{R,i}^4 b_{R,i}(x), \quad x \in (x_{i-1/2}, x_{i+1/2}) \tag{3.38}$$

There are analogous relations for $T(x)$ and $\phi^{\pm}(x)$ over each cell. These expressions are positive as long as the moments are positive, which is true for physical solutions. If the lagged, MC spatial closure produces an outflow from a cell that is negative, then these moments could become negative. In such cases, we force that cell to use a standard lumped relation for the moment equations, with no discontinuity at the outflow, and restart that Newton solve. It is important to note that the spatial closure will still have the same relation between the moments and the outflow; the lumping relation only affects the linear representation that the moments correspond to. For example in Eq. (3.22), the lumped representation changes $2/3T_{L,i} + 1/3T_{R,i}$ to $T_{L,i}$, but no modification are made to the absorption term $\sigma_{a,i}\langle\phi\rangle_{L,i}$.

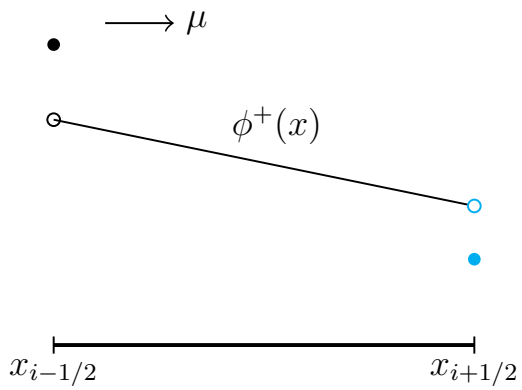

Figure 3.3: Linear doubly-discontinous representation for mean intensity in LO equations.

3.5.4 Issues with ECMC for Spatial Closure

There are several issues with ECMC that cause the LO moments to not exactly preserve the HO moments, even for a linear problem. With ECMC, global and, particularly, local energy balance are generally not preserved. For standard MC, there are source biasing techniques (e.g., systematic sampling) that exactly preserve the local zeroth moment of the source and thus satisfy the local balance equations [31, 43]). However, for our HOLO method, even with standard MC we have to reconstruct the bilnear moment of x and μ, so the consistency terms lead to LO equations that do not exactly preserve the first moment of the HO solution[2]. One final reason is that the analog treatment of absorption for particles below the weight cutoff (e.g., see Sec. 4.4) results in $\sigma_a \phi_i^{HO}$ and the amount of energy removed from a cell during MC transport to not be equal; this is due to statistical noise in the path-length estimators for ϕ_i^{HO}. However, ECMC will preserve balance to the order of the iterative error and statistical noise, so the closure parameters will reproduce the HO moments to

[2]It was verified that with standard MC, systematic sampling, no analog sampling, and a closure that is only a function of the zeroth moment, the LO solution exactly reproduces the HO moments, for a linear problem

the accuracy of the LO solution.

3.6 Test Problems

To investigate the utility of the face closures we compare to the LD spatial closure for two test problems. We are interested in the accuracy of the solution and consistency between the HO and LO solutions, particularly for coarser meshes. The consistency for the (l)-th particular simulation is measured with the relative L_2 norm of the difference between the projected HO and LO solutions, i.e.,

$$\|\phi_{HO} - \phi_{LO}\|_{2,rel}^{(l)} = \frac{\sqrt{\int_0^X \left(\phi_{HO}^{(l)}(x) - \phi_{LO}^{(l)}(x)\right)^2 \mathrm{d}x}}{\sqrt{\int_0^X \left(\phi_{LO}^{(l)}(x)\right)^2 \mathrm{d}x}} \tag{3.39}$$

where $\phi_{LO}(x)$ and $\phi_{HO}(x)$ are the LDFE representations in space of the intensity from the HO and LO solvers, from the end of the last time step. The error between a reference solution and a fine solution for the (l)-th simulation is computed as

$$\|e\|_{2,rel}^{(l)} = \frac{\|\phi_{LO}^{n+1,(l)}(x) - \phi_{LO}^{n+1,ref}\|}{\|\phi_{LO}^{n+1,ref}\|} \tag{3.40}$$

All L_2 norms are computed using quadrature over the finest spatial mesh. An integrated measure of the error in cell-averaged mean intensities on the mesh of the l-th simulation, with $N_c^{(l)}$ spatial cells, is computed as

$$\|e\|_{a,rel}^{(l)} = \left(\frac{\sum_{i=1}^{N_c^{(l)}} \left(\phi_i^{n+1,(l)} - \phi_i^{n+1,ref}\right)^2}{\sum_{i=1}^{N_c^{(l)}} \left(\phi_i^{n+1,ref}\right)^2} \right)^{1/2}, \tag{3.41}$$

where $\phi_i^{n+1,ref}$ is computed by spatially averaging the fine mesh solution over the i-th coarse spatial cell.

The sample mean of each of the above metrics is estimated based on 20 independent simulations; the sample standard deviation for each *mean* is also reported, e.g.,

$$s\left(\|e\|_{2,rel}\right) = \left[\frac{1}{20-1}\sum_{l=1}^{20}\left(\|e\|_{2,rel}^{(l)} - \|e\|_{2,rel}\right)^2\right]^{1/2}, \tag{3.42}$$

where $\|e\|_{2,rel} = \sum_{l=1}^{20}\|e\|_{2,rel}^{(l)}/20$ is the mean.

3.6.1 Smooth Problem

For this problem, the radiation and material energies are initially in equilibrium at 0.01 keV. An isotropic incident intensity of 50 eV is applied at $x = 0$; the incident intensity on the right boundary is 10 eV. The material properties are $\rho = 1$ g cm^{-3}, $c_v = 0.2$ jks/keV-g, and $\sigma_a = 10$ cm^{-1}. The simulation end time is 0.5 sh. The time step size increases by 10% each time step until the maximum step size of 0.01 sh is reached, beginning from $\Delta t = 0.001$ sh. This problem is intended to have less steep gradients in the intensity by having constant constant cross sections, a smaller boundary source, and diffusive problem parameters. The problem has a smaller optical thickness than other problems tested so that the face-based solutions can be efficiently estimated, but the small c_v value makes the solution relatively diffusive. This problem did not require the lumped relation to produce positive solutions. However, when projecting from a refined mesh back to the coarse mesh, it was necessary to rotate the solution to be positive.

All simulations of this problem used 585,900 histories divided over 9 ECMC batches; beginning from 30,000 histories and 10 μ cells, 30% of cells were adaptively refined every third batch, and the number of histories is increased to keep the average

number of histories per cell constant. We have have performed two outer HOLO iterations over each time step for all cases; it was found that additional iterations did not increase consistency, because of the magnitude of statistical noise. Relative convergence of HOLO iterations was below 10^{-3} for two iterations for all cases. Fig. 3.4 compares cell-averaged radiation temperatures for various spatial closures at coarse mesh sizes and a fine-mesh solution. The HO spatial closures curve is for the scaled-slope closure given by Eq. (3.31). There was visually no difference in the results between the scaled-averaged, scaled-slope, or LD closure. A step closure in all cells was inaccurate for this problem.

Table 3.1 compares the different error metrics for different spatial closures and numbers of cells. The reference solution for all calculations was the average of 10 simulations with $N_c = 500$ spatial cells. In all cases, the HO spatial closure produces higher accuracy in the L_2 norms and greater consistency between the solvers. However, there is not an improvement in accuracy of the cell-averaged intensities. Neglecting noise, the LDFE representation can be third order accurate for the $\|e\|_a$ norm and second-order accurate in the L_2 norm [26]. The statistical noise induced in face tallies makes the additional accuracy that the MC transport can use not greater than the benefit of higher spatial integration by the MC transport. It is noted that, overall, there is very low statistical noise in each of these solutions due to the ECMC method and relatively high number of histories; at lower history counts, the small gains of the HO spatial closure will degrade and stability becomes an issue.

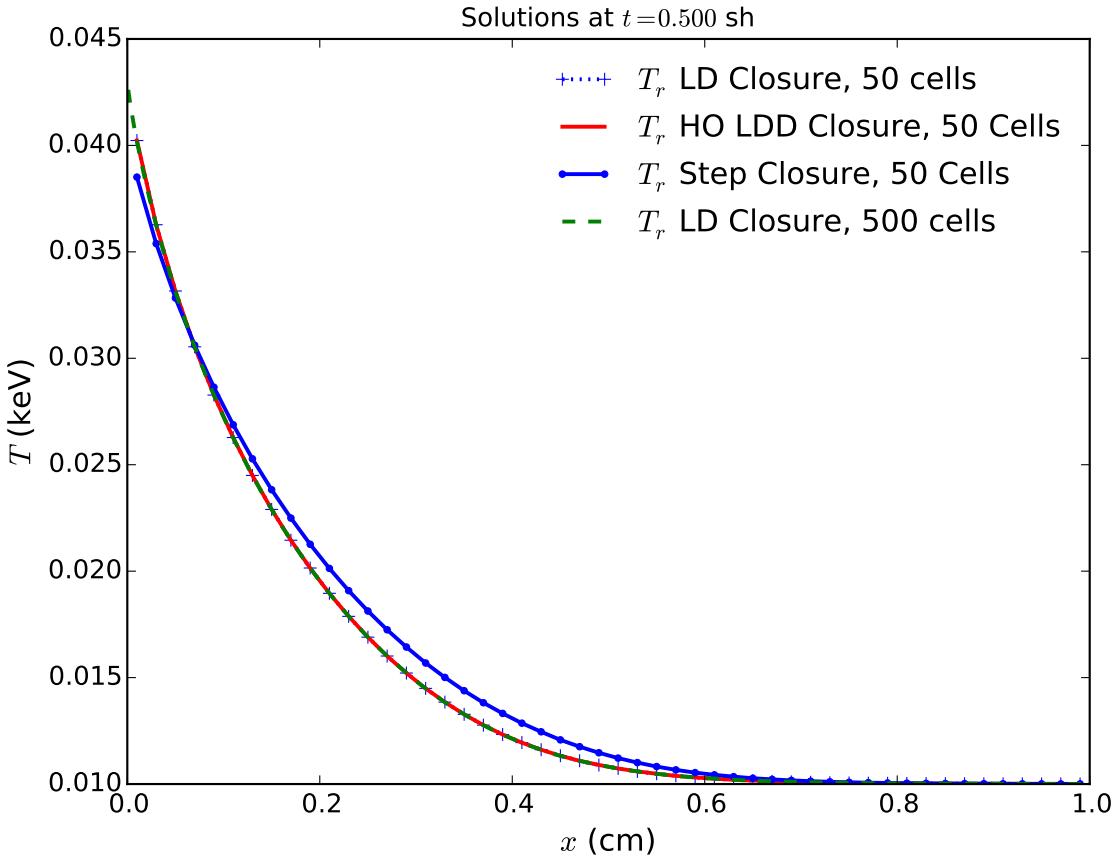

Figure 3.4: Comparison of solutions for different spatial closures.

Table 3.1: Comparison of error metrics, reported as percentages, averaged over 20 simulations of smooth problem. The absolute standard deviation for each value is reported in parenthesis. Reference solution uses 500 cells.

Spatial Closure	$\|e\|_2$	$\|e\|_a$	$\|\phi^{HO} - \phi^{LO}\|_2$
$N_c = 20$ cells			
LDFE	6.60% (0.17%)	2.80% (5.7e-03%)	2.90% (8.1e-03%)
HO: Scaled Slope	6.10% (2.9e-03%)	3.50% (5.8e-03%)	0.021% (8.6e-03%)
HO: Scaled Average	6.10% (2.7e-03%)	3.50% (5.0e-03%)	0.023% (1.1e-02%)
$N_c = 50$ cells			
LDFE	1.60% (7.9e-04%)	0.59% (3.8e-03%)	0.76%) (4.8e-03%)
HO: Scaled Slope	1.40% (1.5e-03%)	0.67% (3.2e-03%)	0.012% (4.0e-03%)
HO: Scaled Average	1.40% (1.5e-3%)	0.67% (3.1e-03%)	0.013% (3.9e-03%)
$N_c = 100$ cells			
LDFE	0.53% (2.1e-03%)	0.15% (2.5e-03%)	0.30%) (9.7e-03%) %
HO: Scaled Slope	0.45% (1.5e-03%)	0.16% (4.6e-03%)	0.012% (4.8e-03%)
HO: Scaled Average	0.45% (1.4e-03%)	0.16% (4.7e-03%)	0.012% (3.6e-03%)

3.7 Two Material Problem

The HO spatial closures were applied to solution of the two material problem detailed in Sec. 5.0.2. For these results, the time step size is increased from 0.001 sh to a maximum step of 0.01 sh by 5% each step, with the final step adjusted to end at 2 sh.

The scaled-slope closure was found to not stably converge, even for 3 batches of 10^6 histories. This coudl be caused the steep gradients at the foot of the wave. As the solution slightly overshoots, the slope changes signs between cells.

APPENDIX A

DERIVATIONS AND EQUATIONS FOR THE LO SYSTEM

A.1 Useful Moment Relations for LO Equations

There are several relations between various moment definitions that are useful in derivation and manipulation of the LO equations. The following are derived for $\phi(x)$, but can be applied to general moments of functions. The volumetric average terms can be eliminated in terms of the L and R moments from the relation $b_{L,i}(x) + b_{R,i}(x) = 1$.

$$\phi_i = \frac{1}{h_i} \int_{x_{i-1/2}}^{x_{i+1/2}} 1 \, \phi(x) \mathrm{d}x \tag{A.1}$$

$$= \frac{1}{h_i} \left(\int_{x_{i-1/2}}^{x_{i+1/2}} b_{L,i}(x)\phi(x)\mathrm{d}x + \int_{x_{i-1/2}}^{x_{i+1/2}} b_{R,i}(x)\phi(x)\mathrm{d}x \right) \tag{A.2}$$

$$= \frac{1}{2} \left(\langle \phi \rangle_{L,i} + \langle \phi \rangle_{R,i} \right) \tag{A.3}$$

A similar relation can be derived for the first moment in space as

$$\phi_{x,i} = \frac{3}{2} \left(\langle \phi \rangle_{R,i} - \langle \phi \rangle_{L,i} \right) \tag{A.4}$$

The above relations can be inverted to derived a relation for the L and R moments in terms of the slope and average moments. These moment expressions are defined purely in terms of integrals, and are independent of the chosen spatial representation

Once a linear relation on the interior has been assumed, there are other useful closures that can be derived. The standard linear interpolatory expansion, for the

positive half-range, is restated here:

$$\phi^+(x) = \phi^+_{L,i} b_{L,i}(x) + \phi^+_{R,i} b_{R,i}(x) \tag{A.5}$$

Using this expansion, one can derive a relation between the outflow from a cell and the hat function moments that is equivalent to the standard LDFE Galerkin method:

$$\phi^+_{i,R} = 2\langle\phi\rangle^+_{R,i} - \langle\phi\rangle^+_{L,i}, \tag{A.6}$$

where for standard LD $\phi^+_{i+1/2} \equiv \phi_{i,R}$. The assumption of a linear relation on the interior of the cell defines the value for $\phi^+_{i,L}$:

$$\phi^+_{i,L} = 2\langle\phi\rangle^+_{L,i} - \langle\phi\rangle^+_{R,i}, \tag{A.7}$$

To eliminate the LO unknowns in a manner that produces the same moments as the LDFE Galerkin method, the following expression can be used for the outflow from a cell

$$\phi^+_{i+1/2} = \phi^+_i + \frac{\phi^+_{x,i}}{3}, \tag{A.8}$$

which in terms of the hat function moments is equivalent to $\phi^+_{i+1/2} = \langle\phi\rangle^+_{R,i}$. Inserting this expression into Eq. (**??**), and using the same definition for the linear representation over the interior of $\phi^+_{i+1/2}(x) = \phi_{L,i} b_{L,i}(x) + \phi_{R,i} b_{R,i}(x)$, will produce an equivalent set of unknowns as a linear discontinuous method with a lumped representation for the radiation. The temperature equation must be independently lumped. This relation preserves the average within a cell but modifies the first moment.

A similar expression produces a lumped-equivalent representation on the interior

of the cell:

$$\phi_{i,R}^{+} = \phi_i^{+} + \frac{\phi_x^{+}}{3}, \tag{A.9}$$

The moment equations are not modified by using this expression, however the interpretation of the moments as a linear representation over the cell has been altered. This allows for us to ensure a lumped representation on the interior while still using the HO solution to eliminate the outflow from the equations.

A.2 Newtons Method for the LO Equations

This section briefly derives the equations for the Newton's method solution to the nonlinear LO equations, with the LDFE representation of the temperatures, based on the approach in [26]. Because we have only considered problems with constant densities and heat capacities, the linearization described below is in terms of temperature T rather than material internal energy, for simplicity. However, the linearization can be formed in terms of internal energy to apply this method to a general equation of state.

To formulate the linear equations for each Newton step, the Planckian source is linearized in the material and radiation equations (Eq. (2.2) & Eq. (2.1)). Application of the first order Taylor expansion in time to the implicit emission source $\sigma_a ac(T^{n+1})^4$, about some temperature T^* at some time $t^* \in [t^n, t^{n+1}]$, yields

$$\sigma_a^{n+1} acT^{4,n+1} \simeq \sigma_a^* ac\left[T^{*4} + (T^{n+1} - T^*)4T^{*3}\right] \tag{A.10}$$

where $\sigma_a^* \equiv \sigma_a(T^*)$. Substitution of this expression into Eq. (2.2) yields

$$\rho c_v \left(\frac{T^{n+1} - T^n}{\Delta t}\right) = \sigma_a^* \phi^{n+1} - \sigma_a^* ac\left[T^{*4} + (T^{n+1} - T^*)4T^{*3}\right]. \tag{A.11}$$

Algebraic manipulation of this equation yields an expression for $T^{n+1} - T^*$:

$$\left(T^{n+1} - T^*\right) = \frac{\frac{\sigma_a^* \Delta t}{\rho c_v}\left[\phi^{n+1} - acT^{*4}\right] + \left(T^n - T^*\right)}{1 + \sigma_a^* ac\Delta t \frac{4T^{*3}}{\rho c_v}}.$$

This expression is substituted back into Eq. (A.10) to form an explicit approximation for the emission source at t^{n+1} as

$$\sigma_a acT^{4,n+1} \simeq \sigma_a^*(1-f^*)\phi^{n+1} + f^*\sigma_a^* acT^{4,n} + \rho c_v \frac{1-f^*}{\Delta t}(T^n - T^*) \tag{A.12}$$

where $f^* = [1 + \sigma_a^* c\Delta t 4aT^{*3}/(\rho c_v)]^{-1}$ is often referred to as the Fleck factor [11].

Next, the above equation is spatially discretized. Application of the L spatial moment yields

$$\begin{aligned}\langle \sigma_a^* acT^{4,n+1}\rangle_{L,i} = \sigma_{ai}^*(1-f_i^*)\langle\phi^{n+1}\rangle_{L,i} + f_i^*\sigma_{ai}^* ac\left(\frac{2}{3}T_{L,i}^{4,n} + \frac{1}{3}T_{R,i}^{4,n}\right) \\ \rho_i c_{vi}\frac{1-f_i^*}{\Delta t}\left[\frac{2}{3}\left(T_{L,i}^n - T_{L,i}^*\right) + \frac{1}{3}\left(T_{R,i}^n - T_{R,i}^*\right)\right],\end{aligned} \tag{A.13}$$

where $T^{4,n}$ and T^n have been assumed LD and f^* is assumed constant over a cell, i.e., $f_i^* \equiv f(T_i^*)$. The error introduced by a constant f^* approaches zero as the non-linearity is converged because T^* approaches T^{n+1}. Based on an estimate for T^*, Eq. (A.13) is an expression for the Planckian emission source in the radiation moment equations with an additional effective scattering source. A similar expression can be derived for $\langle \sigma_{a,i} acT^4\rangle_R$ and the right moment equations. The expressions for the emissions source is substituted into the discrete radiation moment equations, (Eq. (**??**)– (3.21)) to produce a linear system of equations for the new radiation intensity moments (upon closure of the moment equations).

Once the linear equations have been solved for new radiation moments, new temperature unknowns can be estimated. To conserve energy, the same linearization and discretizations used to solve the radiation equation must be used in the material energy equation. Substitution of Eq. (A.13) into the material energy L moment equation, i.e., Eq. (3.22), ultimately yields

$$\frac{2}{3}T_{L,i}^{n+1} + \frac{1}{3}T_{R,i}^{n+1} = \frac{f_i^* \sigma_{ai}^* \Delta t}{\rho c_v}\left[\langle\phi^{n+1}\rangle_{L,i} - ac\left(\frac{2}{3}T_{L,i}^{4,n} + \frac{1}{3}T_{R,i}^{4,n}\right)\right] + (1-f_i^*)\left(\frac{2}{3}T_{L,i}^{*} + \frac{1}{3}T_{R,i}^{*}\right) + f\left(\frac{2}{3}T_{L,i}^{n} + \frac{1}{3}T_{R,i}^{n}\right) \quad \text{(A.14)}$$

A similar expression is produced for the R moment equation. This produces a local matrix equation to solve for new T unknowns.

Based on these equations, iterations on the value of T^* and unknowns ϕ^{n+1} and T^{n+1} can be performed to converge the nonlinearities of the system. The algorithm for solving the LO equations, with iteration index l, is defined as

1. Initialize $T^{*,l}$ unknowns using T^n or the last estimate of T^{n+1} from previous LO solve
2. Build the LO system based on the effective scattering $(1 - f^{*,l})$ and emission terms evaluated using $T^{*,l}$.
3. Solve the linearized LO system to produce a new estimate $\phi^{n+1,l+1}$.
4. Evaluate a new estimate of $T^{n+1,l+1}$ with energy update equations, e.g., Eq. (A.14).
5. $T^{*,l+1} \leftarrow T^{n+1,l+1}$.
6. Repeat 2-5 until $(T^{n+1,l})^4$ and $\phi^{n+1,l}$ are converged.

Convergence is based on the relative L_2 spatial norm of the change in $\phi^{n+1,l}$ and the emission source $\sigma_a ac \left(T^{n+1,l}\right)^4$.

A.2.1 Damped Newton Iterations

The algorithm in the previous section can be modified to improve the stability of convergence by including a fixed damping factor ξ. In this work, the Newton's method is formulated to directly estimate the final solution each step, rather that in terms of the change in the solution between steps. Thus, an intermediate solve based on the algorithm in the previous section is performed, followed by a damped update of the unknowns. The damped Newton's method algorithm is as follows:

1. Choose a damping factor $\xi \in (0, 1)$
2. Initialize $T^{*,l}$ unknowns using T^n or the last estimate of T^{n+1} from previous LO solve.
3. Build the LO system based on the effective scattering $(1 - f^{*,l})$ and emission terms evaluated using $T^{*,l}$.
4. Solve the linearized LO system to produce an estimate $\phi^{n+1,l+1/2}$.
5. Evaluate a new estimate of $T^{n+1,l+1/2}$ with energy update equations, e.g., Eq. (A.14).
6. Compute new temperatures and intensities as

$$\phi^{n+1,l+1} = \phi^{n+1,l} + \xi \left(\phi^{n+1,l+1/2} - \phi^{n+1,l}\right)$$
$$T^{n+1,l+1} = T^{n+1,l} + \xi \left(T^{n+1,l+1/2} - T^{n+1,l}\right)$$

7. $T^{*,l+1} \leftarrow T^{n+1,l}$.

8. Repeat 2-5 until $(T^{n+1,l})^4$ and $\phi^{n+1,l}$ are converged.

A.3 Analytic Error Contribution for LDD Trial Space

In this section, the treatment of the outflow discontinuity residual source and error tallying is detailed. Define the additional error contribution from the face sources at $x_{i+1/2}$ as $\delta\epsilon^{(m)}$. We have chosen to tally the contribution from these sources with MC everywhere except for at $x_{i+1/2}$. Thus, we need to solve for $\delta\epsilon^{(m)}$ at each face $x_{i+1/2}$ and add that contribution to the tallies $\epsilon(x_{i+1/2},\mu)$, which include the contribution from all other sources. The transport equation satisfied by $\delta\epsilon^{(m)}$, for positive μ and effective total cross section $\hat{\sigma}_t$, is

$$\mu\frac{\partial\delta\epsilon^{(m)}}{\partial x}+\hat{\sigma}_t\delta\epsilon^{(m)}=r_{\text{face}}(x^-_{i+1/2})\delta^-(x-x_{i+1/2})+r_{\text{face}}(x^+_{i+1/2})\delta^+(x-x_{i+1/2}) \quad \text{(A.15)}$$

This equation is integrated from $x_{i+1/2}-\alpha$ to $x_{i+1/2}$ to produce

$$\begin{aligned}\mu\delta\epsilon^{(m)}(x_{i+1/2},\mu)-\mu\delta\epsilon^{(m)}(x_{i+1/2}-\alpha,\mu)+&\int_{x_{i+1/2}-\alpha}^{0}\hat{\sigma}_t\delta\epsilon^{(m)}\mathrm{d}x\\ &=r_{\text{face}}(x^-_{i+1/2})+\int_{x_{i+1/2}-\alpha}^{0}r_{\text{face}}(x^+_{i+1/2})\delta^+(x-x_{i+1/2})\mathrm{d}x. \quad \text{(A.16)}\end{aligned}$$

The integral on the right side of the equation is zero because $\delta^+(x-x_{i+1/2})$ is zero for $(-\infty,x_{i+1/2}]$. The limit of the above equation is taken as $\alpha\to 0$, i.e.,

$$\lim_{\alpha\to 0}\left(\mu\delta\epsilon^{(m)}(x_{i+1/2},\mu)-\mu\delta\epsilon^{(m)}(x_{i+1/2}-\alpha,\mu)+\int_{x_{i+1/2}-\alpha}^{0}\hat{\sigma}_t\delta\epsilon^{(m)}\mathrm{d}x\right)=\lim_{\alpha\to 0}r_{\text{face}}(x^-_{i+1/2}) \quad \text{(A.17)}$$

The integral goes to zero because $\delta\epsilon^{(m)}$ is smooth on the interior of the cell, and $\mu\delta\epsilon^{(m)}(x_{i+1/2} - \alpha, \mu)$ goes to zero because there is no source upstream of $x^-_{i+1/2}$. Thus, the final solution is

$$\delta\epsilon^{(m)}(x_{i+1/2}, \mu) = \frac{r_{\text{face}}(x^-_{i+1/2})}{\mu} = \tilde{I}^{(m)}(x^-_{i+1/2}, \mu) - \tilde{I}^{(m)}(x_{i+1/2}, \mu). \tag{A.18}$$

The update equation for $I(x_{i+1/2}, \mu)$ is thus

$$\tilde{I}^{(m+1)}(x_{i+1/2}, \mu) = \tilde{I}^{(m)}(x_{i+1/2}, \mu) + \epsilon^{(m)}(x_{i+1/2}, \mu) + \delta\epsilon^{(m)}(x_{i+1/2}, \mu) \tag{A.19}$$

$$= \tilde{I}^{(m)}(x^-_{i+1/2}, \mu) + \epsilon^{(m)}(x_{i+1/2}, \mu). \tag{A.20}$$

A.4 Analytic Neutronics answer for Source fixup

In this section we model a fixed-source, pure-absorber neutronics calculation where we know the analytic answer to test our fixup. If we make the mesh thick enough, we can set the solution to be the equilibrium answer $\psi(x) = \frac{q(x)}{2\sigma_a}$. For a general isotropic source $Q(x)$, the 1D transport equation to be solved is

$$\mu\frac{\partial\psi}{\partial x} + \sigma_a\psi(x, \mu) = \frac{q(x)}{2} \tag{A.21}$$

with boundary condition $\psi(0, \mu) = \psi_{inc},\ \mu > 0$ and $\psi(x_R, \mu) = \frac{q(x_R)}{2\sigma_a}$ for $\mu < 0$, where x_R is the right boundary. This first order differential equation is solved using an integration factor. The solution to this equation for $\mu > 0$ is given by

$$\psi(x, \mu) = \psi_{inc}e^{\frac{-\sigma_a x}{\mu}} + \int_0^x \frac{q(x')}{2\mu}e^{\frac{-\sigma_a x'}{\mu}}\,\mathrm{d}x', \quad \mu > 0 \tag{A.22}$$

Integration of this result over the positive half range of μ gives

$$\phi^{+}(x) = \psi_{inc}\,\mathrm{E}_2(\sigma_a x) + \frac{1}{2}\int_0^x q(x')\,\mathrm{E}_1(\sigma_a x')\mathrm{d}x'. \tag{A.23}$$

In the simplification of a constant source, the integral reduces to

$$\phi^{+}(x) = \psi_{inc}\,\mathrm{E}_2(\sigma_a x) + \frac{q}{2\sigma_a}\left(1 - \mathrm{E}_2(\sigma_a x)\right). \tag{A.24}$$

Also, for a constant source the solution for the negative half range becomes a constant, i.e.,

$$\phi^{-}(x) = \frac{q}{\sigma_a} \tag{A.25}$$

Combination of the above two equations gives the solution for the scalar flux:

$$\phi(x) = \psi_{inc}\,\mathrm{E}_2(\sigma_a x) + \frac{q}{2\sigma_a}\left(1 - \mathrm{E}_2(\sigma_a x)\right) + \frac{q}{\sigma_a}. \tag{A.26}$$

APPENDIX B

DERIVATION OF THE WLA-DSA EQUATIONS

In this section, we derive the discretized diffusion equation and LD mapping equations that are used in the WLA-DSA equations. To simplify notation, we derive the equations from a generic transport equation (rather than the error equations) with isotropic scattering and source q_0, i.e.,

$$\mu\frac{\partial I}{\partial x} + \sigma_t I = \frac{\sigma_s}{2}\left(\phi(x) + q_0\right). \tag{B.1}$$

B.1 Forming a Continuous Diffusion Equation

First, a continuous spatial discretization of a diffusion equation is derived. The mean intensity ϕ will ultimately be assumed continuous at faces to produce a standard three-point finite-difference diffusion discretization. The zeroth and first μ moment of Eq. (B.1) produce the P_1 equations [22, 38], i.e.,

$$\frac{\partial J}{\partial x} + \sigma_a\phi = q_0 \tag{B.2}$$

$$\sigma_t J + \frac{1}{3}\frac{\partial \phi}{\partial x} = 0. \tag{B.3}$$

The spatial finite element moments (defined by Eq. (3.3) and (**??**)) are taken of the above equations. The mean intensity is assumed linear on the interior of the cell, i.e., $\phi(x) = \phi_L b_L(x) + \phi_R b_R(x)$, for $x \in (x_{i-1/2}, x_{i+1/2})$. Taking the left moment, evaluating integrals, and rearranging yields

$$J_i - J_{i-1/2} + \frac{\sigma_{a,i}h_i}{2}\left(\frac{2}{3}\phi_{L,i} + \frac{1}{3}\phi_{R,i}\right) = \frac{h_i}{2}\langle q\rangle_{L,i}\ , \tag{B.4}$$

where J_i is the average of the flux J over the cell. The moments of q are not simplified to be compatible with the error equations which are in terms of moments. For the R moment

$$J_{i+1/2} - J_i + \frac{\sigma_{a,i} h_i}{2} \left(\frac{2}{3} \phi_{L,i} + \frac{1}{3} \phi_{R,i} \right) = \frac{h_i}{2} \langle q \rangle_{R,i} \ . \tag{B.5}$$

The equation for the L moment is evaluated for cell $i+1$ and added to the R moment equation evaluated at i. The flux J is assumed continuous at $i + 1/2$ to eliminate the face fluxes from the equations. The sum of the two equations becomes

$$J_{i+1} - J_i + \frac{\sigma_{a,i+1} h_{i+1}}{2} \left(\frac{2}{3} \phi_{L,i+1} + \frac{1}{3} \phi_{R,i+1} \right) + \frac{\sigma_{a,i} h_i}{2} \left(\frac{1}{3} \phi_{L,i} + \frac{2}{3} \phi_{R,i} \right) = \frac{h}{2} \left(\langle q \rangle_{L,i+1} + \langle q \rangle_{R,i} \right) . \tag{B.6}$$

The mean intensity is approximated as continuous at each face, i.e., $\phi_{L,i+1} = \phi_{R,i} \equiv \phi_{i+1/2}$. Adding the L and R moments of Eq. (B.3) together, with the continuous approximation for $\phi_{i+1/2}$, produces a discrete Fick's law equation [33]

$$J_i = -D_i \frac{\phi_{i+1/2} - \phi_{i-1/2}}{h_i}, \tag{B.7}$$

where $D_i = 1/(3\sigma_{t,i})$. Substitution of Eq. (B.7) into Eq. (B.6) and rearranging yields the following discrete diffusion equation:

$$\left(\frac{\sigma_{a,i+1} h_{i+1}}{6} - \frac{D_{i+1}}{h_{i+1}} \right) \phi_{i+3/2} + \left(\frac{D_{i+1}}{h_{i+1}} + \frac{D_i}{h_i} + \frac{\sigma_{a,i+1} h_{i+1}}{3} + \frac{\sigma_{a,i} h_i}{3} \right) \phi_{i+1/2} + \left(\frac{\sigma_{a,i} h_i}{6} - \frac{D_i}{h_i} \right) \phi_{i-1/2} = \frac{h_{i+1}}{2} \langle q \rangle_{L,i+1} + \frac{h_i}{2} \langle q \rangle_{R,i} \ . \tag{B.8}$$

To allow for the use of lumped or standard LD in these equations, we introduce the factor θ, with $\theta = 1/3$ for standard LD, and $\theta = 1$ for lumped LD. The diffusion

equation becomes

$$\left(\frac{\sigma_{a,i+1}h_{i+1}}{4}(1-\theta)-\frac{D_{i+1}}{h_{i+1}}\right)\phi_{i+3/2}+\left(\frac{D_{i+1}}{h_{i+1}}+\frac{D_i}{h_i}+\left(\frac{1+\theta}{2}\right)\left[\frac{\sigma_{a,i+1}h_{i+1}}{2}+\frac{\sigma_{a,i}h_i}{2}\right]\right)\phi_{i+1/2}$$
$$+\left(\frac{\sigma_{a,i}h_i}{4}(1-\theta)-\frac{D_i}{h_i}\right)\phi_{i-1/2}=\frac{h_{i+1}}{2}\langle q\rangle_{L,i+1}+\frac{h_i}{2}\langle q\rangle_{R,i}\ . \quad \text{(B.9)}$$

Summation over all cells forms a system of equations for ϕ at each face.

B.1.1 Diffusion Boundary Conditions

The upwinding in the LO system exactly satisfies the inflow boundary conditions, therefore a vacuum boundary condition is applied to the diffusion error equations. The equation for the left moment at the first cell is given by

$$J_1-J_{1/2}+\frac{\sigma_{a,i}h_i}{2}\left(\frac{1+\theta}{2}\phi_{L,i}+\frac{1-\theta}{2}\phi_{R,i}\right)=\frac{h_i}{2}\langle q\rangle_{L,i}\ , \quad \text{(B.10)}$$

The Marshak boundary condition for the vacuum inflow at face $x_{1/2}$ is given as

$$J^+_{1/2}=0=\frac{\phi_{1/2}}{4}+\frac{J_{1/2}}{2}, \quad \text{(B.11)}$$

which can be solved for $J_{1/2}$. Substitution of the above equation and Eq. (B.7) into Eq. (B.10) gives

$$\left(\frac{1}{2}+\sigma_{a,1}h_1\frac{1+\theta}{4}-\frac{D_1}{h_1}\right)\phi_{1/2}+\left(\sigma_{a,1}h_1\frac{1-\theta}{4}-\frac{D_1}{h_1}\right)\phi_{3/2}=\frac{h_i}{2}\langle q\rangle_{L,1} \quad \text{(B.12)}$$

A similar expression can be derived for the right-most cell.

B.2 Mapping Solution onto LD Unknowns

Solution of the continuous diffusion equation will provide an approximation to ϕ on faces, denoted as $\phi^C_{i+1/2}$. We now need to map the face solution onto the LD

representation of ϕ. To do this, first we take the L and R finite element moments of the P_1 equations. A LDFE dependence is assumed on the interior of the cell for J and ϕ. Taking moments of Eq. (B.2) and simplifying yields

$$J_{i+1/2} - \frac{J_{L,i} + J_{R,i}}{2} + \frac{\sigma_{a,i} h_i}{2} \left(\frac{1}{3}\phi_{L,i} + \frac{2}{3}\phi_{R,i} \right) = \frac{h_i}{2} \langle q \rangle_{R,i} \tag{B.13}$$

$$\frac{J_{L,i} + J_{R,i}}{2} - J_{i-1/2} + \frac{\sigma_{a,i} h_i}{2} \left(\frac{2}{3}\phi_{L,i} + \frac{1}{3}\phi_{R,i} \right) = \frac{h_i}{2} \langle q \rangle_{L,i} \tag{B.14}$$

The moment equations for Eq. (B.3) are

$$\frac{1}{3} \left(\phi_{i+1/2} - \frac{\phi_{i,L} + \phi_{i,R}}{2} \right) + \frac{\sigma_{t,i} h_i}{2} \left(\frac{1}{3} J_{L,i} + \frac{2}{3} J_{R,i} \right) = 0 \tag{B.15}$$

$$\frac{1}{3} \left(\frac{\phi_{i,L} + \phi_{i,R}}{2} - \phi_{i-1/2} \right) + \frac{\sigma_{t,i} h_i}{2} \left(\frac{2}{3} J_{L,i} + \frac{1}{3} J_{R,i} \right) = 0 \tag{B.16}$$

The face terms $J_{i\pm1/2}$ and $\phi_{i\pm1/2}$ need to be eliminated from the system. First, the scalar intensity is assumed to be the value provided by the continuous diffusion solution at each face, i.e., $\phi_{i\pm1/2} = \phi^C_{i\pm1/2}$. Then, the fluxes are decomposed into half-range values to decouple the equations between cells. At $x_{i+1/2}$, the flux is composed as $J_{i+1/2} = J^+_{i+1/2} + J^-_{i+1/2}$, noting that in this notation the half-range fluxes are $J^\pm_{i+1/2} = \pm \int_0^\pm \mu I(x_{i+1/2}, \mu) \mathrm{d}\mu$[1]. We approximate the incoming fluxes, e.g., $J^-_{i+1/2}$, based on $\phi^C_{i+1/2}$ and a P_1 approximation. The P_1 approximation provides the following relation [38]

$$\phi = 2(J^+ - J^-). \tag{B.17}$$

At $x_{i+1/2}$, the above expression is solved for the incoming current $J^-_{i+1/2}$. The total

[1]Typically, the half-range fluxes are defined with integrals weighted with $|\mu|$, but this notation would not be consistent with our definition of the half-range consistency terms

current becomes

$$J_{i+1/2} = J^+_{i+1/2} - J^-_{i+1/2} = 2J^+_{i+1/2} - \frac{\phi^C_{i+1/2}}{2}, \tag{B.18}$$

In the positive direction, at the right face, the values of ϕ and J are based on the LD representation within the cell at that face, i.e., $\phi_{R,i}$ and $J_{R,i}$. The standard P_1 approximation for the half-range fluxes is used[33], i.e.,

$$J^\pm = \frac{\gamma\phi}{2} \pm \frac{J}{2}, \tag{B.19}$$

where γ accounts for the difference between the LO parameters and the true P_1 approximation. Thus, for the right face and positive half-range,

$$J^+_{i+1/2} = \frac{\gamma}{2}\phi_{i,R} + \frac{J_{i,R}}{2} \tag{B.20}$$

A similar expression can be derived for $x_{i-1/2}$. The total fluxes at each face are thus

$$J_{i+1/2} = \gamma\phi_{i,R} + J_{i,R} - \frac{\phi^C_{i+1/2}}{2} \tag{B.21}$$

$$J_{i-1/2} = \frac{\phi^C_{i-1/2}}{2} - \gamma\phi_{i,L} + J_{i,L} \tag{B.22}$$

Substitution of these results back into the LD balance equations and introduction of the lumping notation yields the final equations

$$\left(\gamma\phi_{i,R} + J_{i,R} - \frac{\phi^C_{i+1/2}}{2}\right) - \frac{J_{L,i} + J_{R,i}}{2} + \frac{\sigma_{a,i}h_i}{2}\left(\frac{(1-\theta)}{2}\phi_{L,i} + \frac{(1+\theta)}{2}\phi_{R,i}\right) = \frac{h_i}{2}\langle q\rangle_{R,i} \tag{B.23}$$

$$\frac{J_{L,i}+J_{R,i}}{2}-\left(\frac{\phi^C_{i-1/2}}{2}-\gamma\phi_{i,L}+J_{i,L}\right)+\frac{\sigma_{a,i}h_i}{2}\left(\frac{(1+\theta)}{2}\phi_{L,i}+\frac{(1-\theta)}{2}\phi_{R,i}\right)=\frac{h_i}{2}\langle q\rangle_{L,i} \tag{B.24}$$

$$\frac{1}{3}\left(\phi^C_{i+1/2}-\frac{\phi_{i,L}+\phi_{i,R}}{2}\right)+\frac{\sigma_{t,i}h_i}{2}\left(\frac{(1-\theta)}{2}J_{L,i}+\frac{(1+\theta)}{2}J_{R,i}\right)=0 \tag{B.25}$$

$$\frac{1}{3}\left(\frac{\phi_{i,L}+\phi_{i,R}}{2}-\phi^C_{i-1/2}\right)+\frac{\sigma_{t,i}h_i}{2}\left(\frac{(1+\theta)}{2}J_{L,i}+\frac{(1-\theta)}{2}J_{R,i}\right)=0. \tag{B.26}$$

The above equations are completely local to each cell and fully defined, including for boundary cells. For simplicity, we just take $\gamma = 1/2$. The system can be solved for the desired unknowns $\phi_{i,L}$, $\phi_{i,R}$, $J_{i,L}$, and $J_{i,R}$, which represent the mapping of $\phi^C_{i+1/2}$ onto the LD representation for $\phi^{\pm}(x)$.